

From the seep to the surface: the ascent and dissolution of methane bubbles in the ocean

Jiangzhi Chen¹

¹Institute of Deep Sea Science and Engineering, Chinese Academy of Sciences, Sanya, Hainan Province 572000

Key Points:

- a spherical bubble ascent model is developed to estimate the amount of methane gas in the oceans entering the atmosphere
- the model is employed to understand the ocean-air methane exchange in the Shenhua area, South China Sea
- model results are used to quantify the possible outcomes of methane gas leak caused by the dissociation of methane hydrate

arXiv:1802.09162v1 [physics.geo-ph] 26 Feb 2018

Corresponding author: Jiangzhi Chen, chenjz@idsse.ac.cn

Abstract

Methane, as a strong greenhouse gas, has 21–25 times the warming potential per unit mass than carbon dioxide, and the methane from the oceans can contribute to $\sim 4\%$ of the annual atmosphere methane budget. Large methane bubble plumes have been observed in seep sites globally on shallow continental shelves, and emerging industry of methane hydrates mining causes growing environmental concern on possible disastrous blowout which destabilizes the methane hydrate and releases huge amount of methane gas. To better estimate how much methane in gaseous phase leaked from the seeps can reach the atmosphere, a simplified model is developed to simulate the ascent of a methane bubble from a shallow ocean methane seep, and the methane transfer with the surrounding water. The breakup and coalescence of bubbles are neglected, and the bubble is assumed to remain spherical following a vertical path during the whole rising process. We calculated the survival distance of bubbles with varying initial sizes and depths and the remaining percentage of methane reaching the sea surface, and applied the results to the seep sites in the Shenhu area in the South China Sea. The study can provide insight into the relative significance of different water bodies in contributing to the atmosphere greenhouse gas.

1 Introduction

Atmospheric methane (CH_4) is a strong greenhouse gas, with at least 20 times the warming potential per unit mass than that of CO_2 [McGinnis *et al.*, 2006; Leifer, 2010]. Observations have confirmed that the concentration of methane has tripled since preindustrial times [Bousquet *et al.*, 2006], and is increasing fast in the atmosphere [Dlugokencky *et al.*, 2011; Sussmann *et al.*, 2012; Nisbet *et al.*, 2016]. Currently about 64% of methane released to the atmosphere comes from anthropogenic sources (e.g., livestock farming, fossil fuels, and biomass burning), but natural sources (e.g., wetlands, termites, lakes, and oceans) also contribute to about 36% of total methane budget [Bousquet *et al.*, 2006, see supplemental material], among which oceans comprise up to 10% of the natural methane emission, and lakes provide another 10% [Bastviken *et al.*, 2004].

In oceans, methane is produced by microbial activities mainly related to degradation of the organic material in the sediments and serpentinization and iddingsization where hydrogen is produced. Seep sites with large volumes of methane gas leakage have been reported globally via visual and acoustic methods. These sites vary in depth with equivalent methane bubble radii less than 0.5 cm (see Table 1). The small radius may be determined by the sizes

of sediment particles and the methane flux rates. Besides the gaseous and dissolved methane,

Site	Depth (m)	a_e (mm)	Reference
Central Nile Deep Sea Fan	~1650	2.75	<i>Römer et al.</i> [2014]
Håkon Mosby mud volcano (Norway)	1250	2.6	<i>Sauter et al.</i> [2006]
GC-185 in the Gulf of Mexico	525–550	~3	<i>Leifer and MacDonald</i> [2003]
Makran continental margin (Pakistan)	575–2870	2.6	<i>Römer et al.</i> [2012a]
Vodyanitski mud volcano (Black Sea)	2070	2.6	<i>Sahling et al.</i> [2009]
Kerch seep area (Black Sea)	890	2.89	<i>Römer et al.</i> [2012b]
northwestern Black Sea shelf	70–112	2.6	<i>Greinert et al.</i> [2010]
southern summit of Hydrate Ridge, Oregon	780	3–3.5	<i>Rehder et al.</i> [2002]
Utsira High, Central North Sea (Norway)	81–93	1.6–3.7	<i>Vielstädte et al.</i> [2015]

Table 1. Published global seeps sites where methane bubble emission is observed. The depth and equivalent bubble radius are reported here. The depth of sites vary between 70–2870 m, but the bubble radii are all below 4 mm.

there is huge amount of methane ($\sim 10^4$ Gt) stored in ocean sediments in the form of methane hydrate [*Kvenvolden*, 1988]. Recently the economic potential of methane hydrate as a possible energy source has attracted more attention, and several countries have conducted experiments to mine ocean methane hydrate, which causes growing environmental concern on possible disastrous blowout with massive dissociation of methane hydrate and huge methane gas emission, similar to the Deepwater Horizon disaster in the Gulf of Mexico or 22/4b in the North Sea. Besides impacts on global warming, huge methane emission can greatly reduce the ocean pH by means of anaerobic methane oxidation, and destroy the ocean environment [*Dickens et al.*, 1995; *Hesselbo et al.*, 2000]. The positive feedback between global warming and methane hydrate dissociation will further deteriorate the situation [*Thomas et al.*, 2002].

To better quantify the contributions of ocean methane to global warming and estimate the risk of massive methane hydrate dissociation, it is important to understand the methane gas transport in oceans. The remaining percentage of methane in a bubble mainly depends on the initial depth and the size. We developed a simplified model simulating the ascent of a methane bubble from a shallow seep located on a continental shelf, e.g., in the Shenhua area in the South China Sea, and model the methane transfer with the surrounding seawater. The

split and coalescence of bubbles are neglected, and bubbles are assumed to remain spherical following vertical paths during the whole ascent. We calculated the survival distance of bubbles with varying initial sizes and depths, and the percentage of methane remained when bubbles reach the ocean surface.

2 Regional setting

Shenhu area, near the Pearl River Mouth Basin in the northern continental margin of the South China Sea, has been recognized as a promising place of gas hydrate extraction due to its relatively high hydrate saturation. Particularly, samples collected from the Shenhu area contain high saturation hydrates (the fraction of pore spaces occupied by gas hydrates) up to 45 % [Wang *et al.*, 2011], drastically higher than that of some other ocean gas hydrate sites where the saturations are only 1–8 % [Davie and Buffett, 2001, 2003]. These samples were discovered in fine-grained sediments about 1200 mbsf. In May, 2017, China successfully extracted gas from the hydrates in a series of production runs in this region, and it is reasonable to believe that more further field explorations will be conducted here, so we apply our model to the Shenhu area to calculate the survival time and distance of methane bubbles.

Taking into account the seasonal change caused by the monsoon, the water temperature and methane concentration near the Shenhu area vary with months. We extract the temperature profile from the SCSPD14 database [Zeng *et al.*, 2016] at a location 19.75° N, 115° E, in the month of July to be consistent with the methane measurement. Figure 1(a) shows the study site, and (b) shows the in situ temperature measurement. The methane concentration profile (c) was measured near the study site in July 2005 by Tseng *et al.* [2017]. It is notable that the methane concentration is high throughout the depth, approximately 7 nM compared with 2–6 nM in the Atlantic and Pacific Oceans [Reeburgh, 2007], possibly due to methane seeps underneath.

3 Modeling approach

The size of the methane bubble is essential to its survival. Decompression during the ascent enlarges the bubble, while the mass transfer to the surrounding seawater reduces the size. For simplicity, the water is treated as stagnant with no upwelling and turbidity currents, and the pressure is hydrostatic. Bubbles are small and sparse enough so the effect of splitting, merging, and turbulence can be neglected. Another assumption is that the bubble remains spherical, and rises vertically. The physical parameters determining the terminal ve-

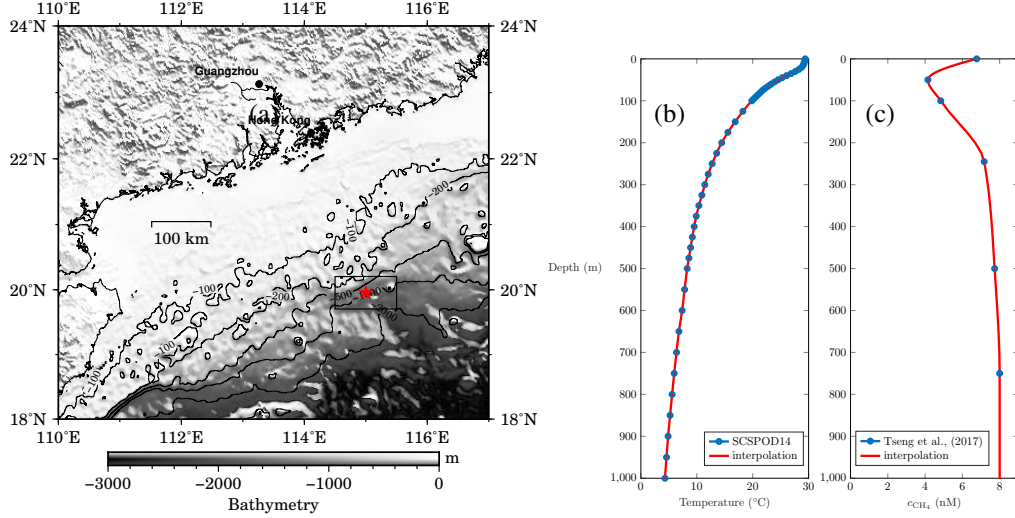


Figure 1. (a): the Shenhu area near the Pearl River Mouth Basin, where the star denotes the study site. The temperature of the study site (b) shows that at about 1 km depth, the temperature drops to around 5 °C, and the dissolved methane concentration (c) plateaus at a high level around 8 nM. The temperature and the methane concentration profiles are interpolated with piecewise cubic Hermite interpolating polynomials.

locity U of a rising methane bubble with a radius a are the densities of the water ρ and the methane gas $\rho' = (1 - \beta)\rho$, the viscosity of the water μ , the surface tension γ , and the gravity g . The viscosity of methane gas inside the bubble is negligible compared to the water viscosity, but at large depth the gas density may not be ignored. The transfer of methane across the bubble interface is dependent on the diffusion coefficient D and Henry's law constant H . The physical parameters are summarized below in Table 2. The parameters of water depend on the temperature, but the temperature range in our model is only 0–30 °C. Within this range, the surface tension and water density change very small and can be treated as constant, while the viscosity can be calculated using the empirical relation [Straus and Schubert, 1977]

$$\mu(T) = \mu_0 \exp\left(\frac{A}{T - B}\right) \quad (1)$$

where $\mu_0 = 2.414 \times 10^{-5} \text{ Pa} \cdot \text{s}$, $A = 570.58 \text{ K}$ and $B = 140 \text{ K}$. The kinematic viscosity of water is $\nu(T) = \mu(T)/\rho$.

3.1 Dimensional analysis

From the physical parameters above, some requirements can be obtained if the bubble rises vertically and remains spherical. The main forces at play are the water resistance $F_i \sim$

Model parameters		Value	
methane gas	molar mass	M [g/mol]	16.04
	diffusion coefficient	D [m ² /s]	1.49×10^{-9}
	Henry's law constant	H [mol/(Pa · m ³)]	1.4×10^{-5}
	van der Waals constants	A [bar · L ² /mol ²]	2.303
B [L/mol]		0.0431	
water	density	ρ [kg/m ³]	$\sim 10^3$
	dynamic viscosity	μ [mPa · s]	0.85 – 1.8
	surface tension	γ [N/m]	~ 0.07

Table 2. Nominal parameter values of the methane gas and seawater. The diffusion coefficient is from *Cussler* [2009], the van der Waals constants are from *Poling et al.* [2001], and the Henry's law constant is from *Sander* [2015].

$\rho U^2 d^2$ where $d = 2a$, the buoyancy force $F_b \sim g \Delta \rho d^3 = g \rho \beta d^3$, the viscous force $F_\mu \sim \mu d U$, and the surface tension force $F_\gamma \sim \gamma d$. From these forces we construct dimensionless parameters including the Reynolds number $Re = F_i/F_\mu = U d/\nu$ and the Weber number $We = F_i/F_\gamma = \rho U^2 d/\gamma$. We can also obtain the Morton number $Mo \equiv g \mu^4/\rho \gamma^3 \sim 10^{-10}$, which is the only dimensionless number specific to the water. According to *Harper* [1972], with small Mo , for impure liquids such as the seawater, the marginal instability should occur at $We < 3$ and $Re \approx 200$, which suggests the maximum stable terminal velocity

$$U_{\text{stable}} < \frac{\gamma We}{\mu Re} \approx 0.58 \text{ m/s.} \quad (2)$$

On the other hand, if the bubble remains spherical, the surface tension force must outweigh the buoyancy force, or the Bond number $Bo = F_b/F_\gamma \equiv \rho \beta g d^2/\gamma \leq 1$, which requires a bubble diameter

$$d \leq \sqrt{\frac{\gamma}{g \beta \rho}} \quad (3)$$

while for a rising bubble, the buoyancy force must be greater than the water resistance, or the Froude number $Fr = F_i/F_b \leq 1$,

$$d \geq \frac{U^2}{g \beta}. \quad (4)$$

Therefore, if a bubble satisfying the assumptions exists, it is necessary that the two inequalities are compatible, which gives another upper bound of the terminal velocity

$$U \leq \left(\frac{\beta g \gamma}{\rho} \right)^{1/4}. \quad (5)$$

This velocity, similar to the average drift velocity in two-phase bubbly flows [Ishii and Zuber, 1979] with a difference of a factor of $\sqrt{2}$, is smaller than U_{stable} and agrees with the in situ measurements at seep sites [Greinert et al., 2006; McGinnis et al., 2006; Sauter et al., 2006; Sahling et al., 2009; Leifer, 2010; Römer et al., 2012a; Wang et al., 2016], so we set the maximum terminal velocity in our model to

$$U_{\text{max}} = \sqrt{2} \left(\frac{\beta g \gamma}{\rho} \right)^{1/4} \approx 0.23 \text{ m/s}. \quad (6)$$

3.2 Methane exchange during ascent

The terminal velocity and mass transfer of a bubble in water has been extensively studied (e.g., [Clift et al., 2005]). The correlation of the terminal velocity and the spherical bubble radius can be better expressed by the value of Re and the drag coefficient C_d , and the terminal velocity is calculated by

$$U = \sqrt{\frac{8ga\beta}{3C_d}}. \quad (7)$$

Numerous experiments have been performed to obtain better correlations [Clift et al., 2005, Table 5.2] within different ranges of Re , and a unified fit for $\text{Re} < 3 \times 10^5$ was proposed by Zhang and Xu [2003]

$$C_d = \frac{24}{\text{Re}} \left(1 + 0.15\text{Re}^{0.687} \right) + \frac{0.42}{1 + 42500\text{Re}^{-1.16}} \quad (8)$$

and the equation agrees exceedingly well with the experimental data by Dioguardi et al. [2017]. For stable ascent with a maximum velocity U_{max} , the rising velocity is modified to

$$U_{\text{unified}} = \frac{1}{\sqrt{U^{-2} + U_{\text{max}}^{-2}}} = \sqrt{\frac{8ga\beta}{3C_d + 2\sqrt{\text{Bo}}}}. \quad (9)$$

When a single spherical bubble of a radius a rises in the ocean with a velocity U , and a diffusion coefficient D , the Péclet number is calculated by

$$\text{Pe} = \frac{2aU}{D} \quad (10)$$

and the mass transfer coefficient k is

$$k = \frac{\text{Sh}D}{2a}. \quad (11)$$

where the Sherwood number Sh depends on the bubble size and velocity. *Zhang and Xu* [2003] proposed a unified equation for $Re < 10^5$ based on previous piecewise correlations [*Clift et al.*, 2005, Eq. 3-49, 5-25, and Table 5.4]

$$Sh = 1 + (1 + Pe)^{1/3} \left(1 + \frac{0.096Re^{1/3}}{1 + 7Re^{-2}} \right) \quad (12)$$

The amount of methane transferred can be determined by

$$\frac{dn}{dt} = 4\pi a^2 k(c_0 - Hp) \quad (13)$$

where c_0 is the concentration of the dissolved methane in the ocean, and the pressure is

$$p = p_0 + \rho gz + \frac{2\gamma}{a}. \quad (14)$$

The methane in the bubble is treated as van der Waals gas due to the high pressure

$$\left(p + \frac{An^2}{V^2} \right) (V - nB) = nRT \quad (15)$$

with the constants $A = 2.303 \text{ bar} \cdot \text{L}^2/\text{mol}^2$ and $B = 0.0431 \text{ L/mol}$ [*Poling et al.*, 2001].

The critical pressure for methane is $p_c = A/27B^2 = 4.6 \text{ MPa}$, equivalent to a water pressure $\sim 460 \text{ mbsf}$. The critical temperature is $T_c = 8A/27RB = 190 \text{ K}$, so the methane remains gaseous, and the gas density in the bubble is related to the molar mass M by $\rho' = nM/V$.

The bubble vertical motion can be described by

$$\frac{dz}{dt} = -U. \quad (16)$$

We numerically solve the equations above, and calculate the amount of methane gas remained for those bubbles that make to the surface.

4 Results and discussion

4.1 Rising of the methane bubble

We simulated the ascent of bubbles released at depths between 200–1000 m, with a initial radius between 1–10 mm using the temperature and methane concentration for the Shenhu area. Figure 2a shows the ratio of the final bubble radius to the initial bubble radius $a_{\text{top}}/a_{\text{initial}}$, and Figure 2b shows the ratio of remaining methane $n_{\text{top}}/n_{\text{initial}}$ of the methane bubbles. Very small bubbles are not likely to reach the surface. For example, a bubble with a radius of 2 mm rising from 200 m depth will lose about 90 % of the methane when it reaches

the atmosphere. Large bubbles, however, will retain more gas, and the expansion is significant due to the decompression. A bubbles with a initial radius over 8 mm rising from depths between 450–700 m can expand as many as four times in the radius when it makes to the surface.

4.2 Instability of bubble rising path

The velocity of a large bubble increases as it expands, and the Reynolds number Re can grow large enough that the assumptions of stable ascent become invalid, and the rising path no longer maintains stable. A bubble with a radius of 9 mm rising at the terminal speed of $U \approx 0.16$ m/s in the water of 27 °C corresponds to $Re \sim 3.3 \times 10^3$, and $We \approx 3.2$, greater than the criteria of marginal stability $We < 3$ and $Re \approx 200$ [Harper, 1972]. Because the bubble is unlikely to grow beyond 5 cm in the radius in our simulation, which corresponds to a Galilei number $Ga \equiv \sqrt{gaa}/\nu \sim 40$ as the transition to oscillatory ellipsoidal or spherical caps according to Tripathi *et al.* [2015], the bubbles are still spherical, but they may split into smaller bubbles.

4.3 Formation of methane hydrate shells

Within the gas hydrate stability zone (GHSZ), a coating of hydrate shell encapsulates the methane bubble [Maini and Bishnoi, 1981; Rehder *et al.*, 2002], and exists until top of the stability zone is reached [Rehder *et al.*, 2002; Warzinski *et al.*, 2014]. The top limit of the GHSZ can be determined by the intersection of the methane phase equilibrium curve [see data compiled by Sloan and Koh, 2007] and the temperature profile (Figure 3). When the hydrate shell forms, water filters through the porous shell, and increases the total mass of the bubble-converted droplet [Ribeiro and Lage, 2008]. The shell also provides additional pressure to the gas within, so the droplet does not expand as a bubble should. As a result, the hydrate shell will help to keep more methane in the bubble.

4.4 Non-ideal gas

The methane gas is treated as van der Waals gas in our simulation, but the equation of state of methane under large pressure is much more complicated. It is possible to use a more sophisticated equation of state such as the model proposed by Peng and Robinson [1976], but since the temperature is around 0 °C $\gg T_c = 190$ K, the deviation is very small. Also,

we assume constant diffusion coefficient, surface tension and Henry's law constant, but it is possible that these parameters also change as the methane becomes non-ideal.

4.5 Turbidity current and upwelling flux

We treated the seawater as stagnant with no motion, however, the water movement is nowhere near stillness due to upwelling fluxes from underneath and turbidity currents from the continental slope. These flows will disturb the water body, and enhanced mixture from the flows will facilitate the dissolution of the methane gas, and reduce the amount of methane reaching the atmosphere.

5 Conclusion

We simulated the ascent of methane bubbles in the Shenhu area, and calculated the amount of methane that reaches the atmosphere. Our simulation shows that for the Shenhu area, methane gas emitted from deep sites >1 km is not likely to reach the ocean surface, as indicated in Figure 2, as long as the bubble radius is smaller than 5 mm. Hydrate-coated bubbles can survive longer and retain more methane, but still small bubbles cannot make through the water column. Kilometers of water column is very effective in keeping the methane in the water body, and a gas blowout will not result in an abrupt amount of methane entering the atmosphere. However, elevated methane emission will lead to larger bubbles, and as the excessive methane is dissolved in shallower water, subsequent anaerobic methane oxidation will change the distribution of pH, which has negative impact on the ocean ecology. Small bubbles with radii 2–3 mm released between 200–1000 m will entirely dissolve in the ocean, and large bubbles over 5 mm rising from 500 m depth can keep at least 40 % when it makes to the ocean surface. In our study area, the top of gas hydrate stability zone lies at about 600 m, so a methane bubble released below this depth can survive longer distance and transfer more methane to shallower depths.

Acknowledgments

= enter acknowledgments here =

References

Bastviken, D., J. Cole, M. Pace, and L. Tranvik (2004), Methane emissions from lakes: Dependence of lake characteristics, two regional assessments, and a global estimate, *Global*

- Biogeochem. Cycles*, 18(4), GB4009, doi:10.1029/2004gb002238.
- Bousquet, P., P. Ciais, J. B. Miller, E. J. Dlugokencky, D. A. Hauglustaine, C. Prigent, G. R. V. der Werf, P. Peylin, E.-G. Brunke, C. Carouge, R. L. Langenfelds, J. Lathière, F. Papa, M. Ramonet, M. Schmidt, L. P. Steele, S. C. Tyler, and J. White (2006), Contribution of anthropogenic and natural sources to atmospheric methane variability, *Nature*, 443(7110), 439–443, doi:10.1038/nature05132.
- Clift, R., J. R. Grace, and M. E. Weber (2005), *Bubbles, drops, and particles*, Courier Corporation.
- Cussler, E. L. (2009), *Diffusion Mass Transfer in Fluid Systems*, Cambridge Series in Chemical Engineering, 3 ed., Cambridge University Press.
- Davie, M. K., and B. A. Buffett (2001), A numerical model for the formation of gas hydrate below the seafloor, *J. Geophys. Res. Solid Earth*, 106(B1), 497–514, doi:10.1029/2000jb900363.
- Davie, M. K., and B. A. Buffett (2003), Sources of methane for marine gas hydrate: inferences from a comparison of observations and numerical models, *Earth Planet. Sci. Lett.*, 206(1-2), 51–63, doi:10.1016/s0012-821x(02)01064-6.
- Dickens, G. R., J. R. O'Neil, D. K. Rea, and R. M. Owen (1995), Dissociation of oceanic methane hydrate as a cause of the carbon isotope excursion at the end of the Paleocene, *Paleoceanography*, 10(6), 965–971, doi:10.1029/95pa02087.
- Dioguardi, F., D. Mele, and P. Dellino (2017), A new one-equation model of fluid drag for irregularly-shaped particles valid over a wide range of Reynolds number, *J. Geophys. Res. Solid Earth*, doi:10.1002/2017jb014926.
- Dlugokencky, E. J., E. G. Nisbet, R. Fisher, and D. Lowry (2011), Global atmospheric methane: budget, changes and dangers, *Philos. Trans. R. Soc. London, Ser. A*, 369(1943), 2058–2072, doi:10.1098/rsta.2010.0341.
- Greinert, J., Y. Artemov, V. Egorov, M. Debatist, and D. McGinnis (2006), 1300-m-high rising bubbles from mud volcanoes at 2080m in the Black Sea: Hydroacoustic characteristics and temporal variability, *Earth Planet. Sci. Lett.*, 244(1-2), 1–15, doi:10.1016/j.epsl.2006.02.011.
- Greinert, J., D. F. McGinnis, L. Naudts, P. Linke, and M. D. Batist (2010), Atmospheric methane flux from bubbling seeps: Spatially extrapolated quantification from a Black Sea shelf area, *J. Geophys. Res.*, 115(C1), doi:10.1029/2009jc005381.

- Harper, J. (1972), The Motion of Bubbles and Drops Through Liquids, *Adv. Appl. Mech.*, *12*, 59–129.
- Hesselbo, S. P., D. R. Gröńcke, H. C. Jenkyns, C. J. Bjerrum, P. Farrimond, H. S. M. Bell, and O. R. Green (2000), Massive dissociation of gas hydrate during a Jurassic oceanic anoxic event, *Nature*, *406*(6794), 392–395, doi:10.1038/35019044.
- Ishii, M., and N. Zuber (1979), Drag coefficient and relative velocity in bubbly, droplet or particulate flows, *AIChE J.*, *25*(5), 843–855, doi:10.1002/aic.690250513.
- Kvenvolden, K. A. (1988), Methane hydrate—A major reservoir of carbon in the shallow geosphere?, *Chem. Geol.*, *71*(1-3), 41–51, doi:10.1016/0009-2541(88)90104-0.
- Leifer, I. (2010), Characteristics and scaling of bubble plumes from marine hydrocarbon seepage in the Coal Oil Point seep field, *J. Geophys. Res.*, *115*(C11), doi:10.1029/2009jc005844.
- Leifer, I., and I. MacDonald (2003), Dynamics of the gas flux from shallow gas hydrate deposits: interaction between oily hydrate bubbles and the oceanic environment, *Earth Planet. Sci. Lett.*, *210*(3-4), 411–424, doi:10.1016/s0012-821x(03)00173-0.
- Maini, B. B., and P. Bishnoi (1981), Experimental investigation of hydrate formation behaviour of a natural gas bubble in a simulated deep sea environment, *Chem. Eng. Sci.*, *36*(1), 183–189, doi:10.1016/0009-2509(81)80062-0.
- McGinnis, D. F., J. Greinert, Y. Artemov, S. E. Beaubien, and A. Wåijest (2006), Fate of rising methane bubbles in stratified waters: How much methane reaches the atmosphere?, *J. Geophys. Res.*, *111*(C9), doi:10.1029/2005jc003183.
- Nisbet, E. G., E. J. Dlugokencky, M. R. Manning, D. Lowry, R. E. Fisher, J. L. France, S. E. Michel, J. B. Miller, J. W. C. White, B. Vaughn, P. Bousquet, J. A. Pyle, N. J. Warwick, M. Cain, R. Brownlow, G. Zazzeri, M. Lanoisellé, A. C. Manning, E. Gloor, D. E. J. Worthy, E.-G. Brunke, C. Labuschagne, E. W. Wolff, and A. L. Ganesan (2016), Rising atmospheric methane: 2007-2014 growth and isotopic shift, *Global Biogeochem. Cycles*, *30*(9), 1356–1370, doi:10.1002/2016gb005406.
- Peng, D.-Y., and D. B. Robinson (1976), A New Two-Constant Equation of State, *Ind. Eng. Chem. Fundam.*, *15*(1), 59–64, doi:10.1021/i160057a011.
- Poling, B. E., J. M. Prausnitz, J. P. O’connell, et al. (2001), *The properties of gases and liquids*, vol. 5, McGraw-hill New York.
- Reeburgh, W. S. (2007), Oceanic Methane Biogeochemistry, *Chem. Rev.*, *107*(2), 486–513, doi:10.1021/cr050362v.

- Rehder, G., P. W. Brewer, E. T. Peltzer, and G. Friederich (2002), Enhanced lifetime of methane bubble streams within the deep ocean, *Geophys. Res. Lett.*, *29*(15), 21–1–21–4, doi:10.1029/2001gl013966.
- Ribeiro, C. P., and P. L. Lage (2008), Modelling of hydrate formation kinetics: State-of-the-art and future directions, *Chem. Eng. Sci.*, *63*(8), 2007–2034, doi:10.1016/j.ces.2008.01.014.
- Römer, M., H. Sahling, T. Pape, G. Bohrmann, and V. Spieß (2012a), Quantification of gas bubble emissions from submarine hydrocarbon seeps at the Makran continental margin (offshore Pakistan), *J. Geophys. Res. Oceans*, *117*(C10), C10,015, doi:10.1029/2011jc007424.
- Römer, M., H. Sahling, T. Pape, A. Bahr, T. Feseker, P. Wintersteller, and G. Bohrmann (2012b), Geological control and magnitude of methane ebullition from a high-flux seep area in the Black Sea—the Kerch seep area, *Mar. Geol.*, *319–322*, 57–74, doi:10.1016/j.margeo.2012.07.005.
- Römer, M., H. Sahling, T. Pape, C. dos Santos Ferreira, F. Wenzhöfer, A. Boetius, and G. Bohrmann (2014), Methane fluxes and carbonate deposits at a cold seep area of the Central Nile Deep Sea Fan, Eastern Mediterranean Sea, *Mar. Geol.*, *347*, 27–42, doi:10.1016/j.margeo.2013.10.011.
- Sahling, H., G. Bohrmann, Y. G. Artemov, A. Bahr, M. BrÄijning, S. A. Klapp, I. Klaucke, E. Kozlova, A. Nikolovska, T. Pape, A. Reitz, and K. Wallmann (2009), Vodyanitskii mud volcano, Sorokin trough, Black Sea: Geological characterization and quantification of gas bubble streams, *Mar. Pet. Geol.*, *26*(9), 1799–1811, doi:10.1016/j.marpetgeo.2009.01.010.
- Sander, R. (2015), Compilation of Henry’s law constants (version 4.0) for water as solvent, *Atmos. Chem. Phys.*, *15*(8), 4399–4981, doi:10.5194/acp-15-4399-2015.
- Sauter, E. J., S. I. Muyakshin, J.-L. Charlou, M. SchlÄijter, A. Boetius, K. Jerosch, E. Damm, J.-P. Foucher, and M. Klages (2006), Methane discharge from a deep-sea submarine mud volcano into the upper water column by gas hydrate-coated methane bubbles, *Earth Planet. Sci. Lett.*, *243*(3–4), 354–365, doi:10.1016/j.epsl.2006.01.041.
- Sloan, E. D., and C. Koh (2007), *Clathrate hydrates of natural gases*, CRC press.
- Straus, J. M., and G. Schubert (1977), Thermal convection of water in a porous medium: Effects of temperature- and pressure-dependent thermodynamic and transport properties, *J. Geophys. Res.*, *82*(2), 325–333, doi:10.1029/jb082i002p00325.

- Sussmann, R., F. Forster, M. Rettinger, and P. Bousquet (2012), Renewed methane increase for five years (2007–2011) observed by solar FTIR spectrometry, *Atmos. Chem. Phys.*, *12*(11), 4885–4891, doi:10.5194/acp-12-4885-2012.
- Thomas, D. J., J. C. Zachos, T. J. Bralower, E. Thomas, and S. Bohaty (2002), Warming the fuel for the fire: Evidence for the thermal dissociation of methane hydrate during the Paleocene-Eocene thermal maximum, *Geology*, *30*(12), 1067, doi:10.1130/0091-7613(2002)030<1067:wtf>2.0.co;2.
- Tripathi, M. K., K. C. Sahu, and R. Govindarajan (2015), Dynamics of an initially spherical bubble rising in quiescent liquid, *Nat. Commun.*, *6*, 6268, doi:10.1038/ncomms7268.
- Tseng, H.-C., C.-T. A. Chen, A. V. Borges, T. A. DelValls, and Y.-C. Chang (2017), Methane in the South China Sea and the Western Philippine Sea, *Cont. Shelf Res.*, *135*, 23–34, doi:10.1016/j.csr.2017.01.005.
- Vielstädte, L., J. Karstens, M. Haeckel, M. Schmidt, P. Linke, S. Reimann, V. Liebetrau, D. F. McGinnis, and K. Wallmann (2015), Quantification of methane emissions at abandoned gas wells in the Central North Sea, *Mar. Pet. Geol.*, *68*, 848–860, doi:10.1016/j.marpetgeo.2015.07.030.
- Wang, B., S. A. Socolofsky, J. A. Breier, and J. S. Seewald (2016), Observations of bubbles in natural seep flares at MC 118 and GC 600 using in situ quantitative imaging, *J. Geophys. Res. Oceans*, *121*(4), 2203–2230, doi:10.1002/2015jc011452.
- Wang, X., D. R. Hutchinson, S. Wu, S. Yang, and Y. Guo (2011), Elevated gas hydrate saturation within silt and silty clay sediments in the Shenhu area, South China Sea, *J. Geophys. Res. Solid Earth*, *116*(B5), doi:10.1029/2010jb007944.
- Warzinski, R. P., R. Lynn, I. Haljasmaa, I. Leifer, F. Shaffer, B. J. Anderson, and J. S. Levine (2014), Dynamic morphology of gas hydrate on a methane bubble in water: Observations and new insights for hydrate film models, *Geophys. Res. Lett.*, *41*(19), 6841–6847, doi:10.1002/2014gl061665.
- Zeng, L., D. Wang, J. Chen, W. Wang, and R. Chen (2016), SCSPD14, a South China Sea physical oceanographic dataset derived from in situ measurements during 1919-2014, *Sci. Data*, *3*, 160,029, doi:10.1038/sdata.2016.29.
- Zhang, Y., and Z. Xu (2003), Kinetics of convective crystal dissolution and melting, with applications to methane hydrate dissolution and dissociation in seawater, *Earth Planet. Sci. Lett.*, *213*(1-2), 133–148, doi:10.1016/s0012-821x(03)00297-8.

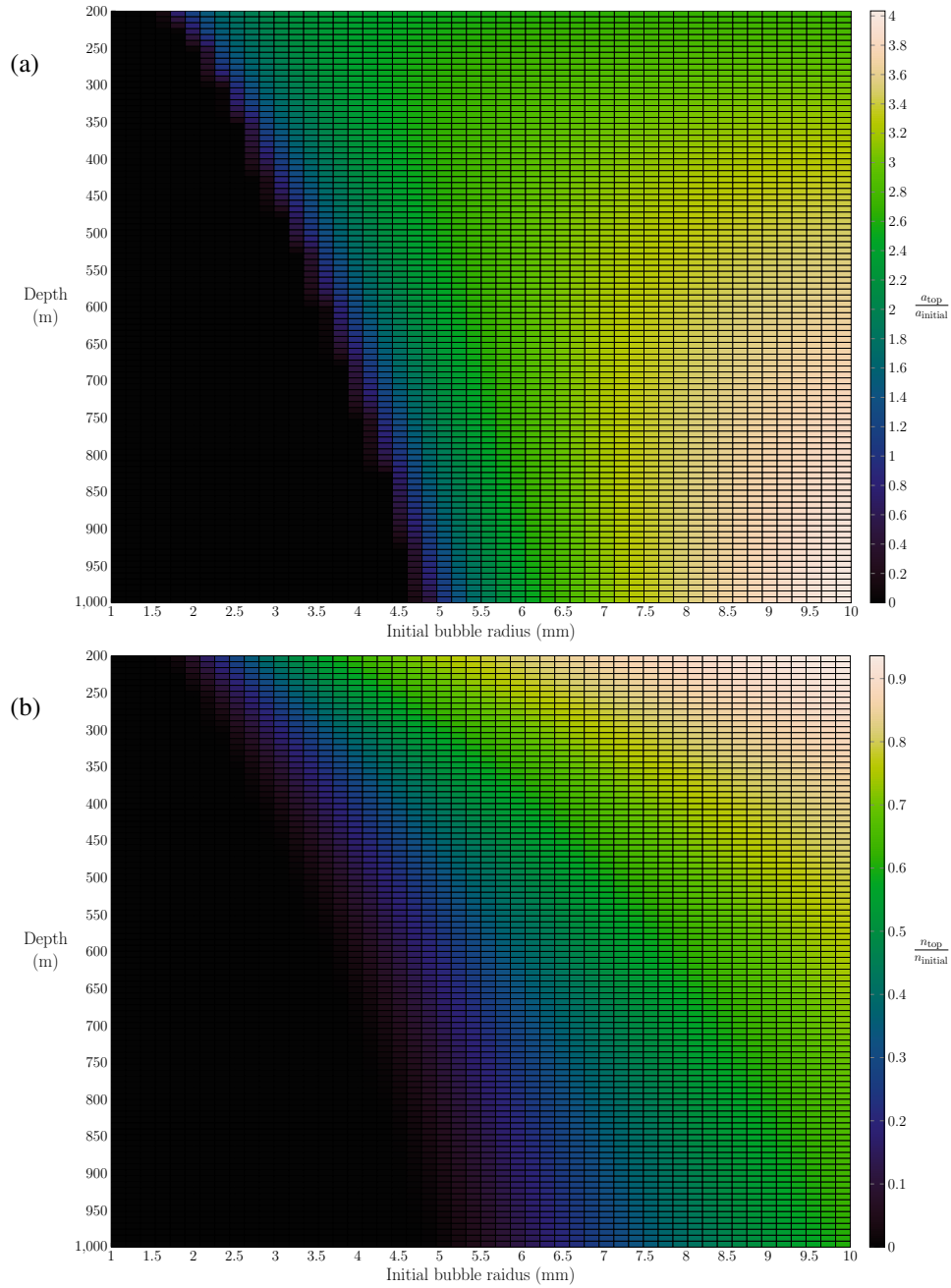


Figure 2. (a) The ratio of the radius of the final bubble reaching the atmosphere to the initial bubble radius. (b) The ratio of the remaining methane gas reaching the atmosphere. In shallow water in the Shenhu area, a large bubble can expand to almost four times in the radius, and bring more than 90 % of the initial methane gas to the atmosphere.

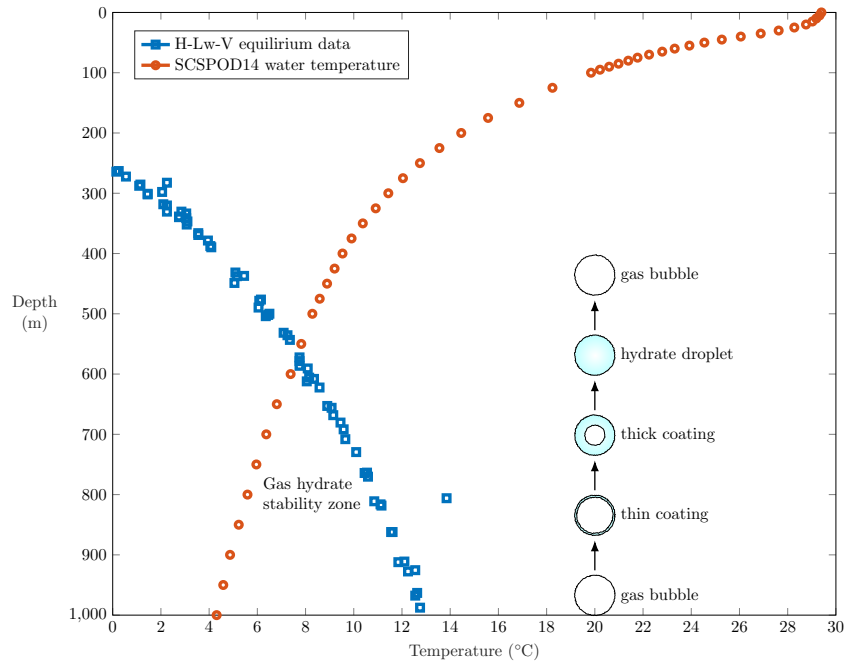


Figure 3. The gas hydrate stability zone in the Shenhu area bounded by the phase equilibrium curve and the SCSP0D14 water temperature profile. The top of GHSZ in our study site is at about 600 m. A schematic shows the formation and dissociation of the hydrate shell around the methane bubble when it rises through the GHSZ.